

Error Mitigation, Optimization, and Extrapolation on a Trapped Ion Testbed

Oliver G. Maupin,¹ Ashlyn D. Burch,² Christopher G. Yale,² Brandon Ruzic,² Antonio Russo,² Daniel S. Lobser,² Melissa C. Revelle,² Matthew N. Chow,^{2,3} Susan M. Clark,² Andrew J. Landahl,^{2,3} and Peter J. Love^{1,4}

¹*Department of Physics and Astronomy, Tufts University, Medford, MA, 02155, USA*

²*Sandia National Laboratories, Albuquerque, NM, 87185, USA*

³*Department of Physics and Astronomy, University of New Mexico, Albuquerque, NM, 87131, USA*

⁴*Computational Science Initiative, Brookhaven National Laboratory, Upton, NY, 11973, USA*

Current noisy intermediate-scale quantum (NISQ) trapped-ion devices are subject to errors which can significantly impact the accuracy of calculations if left unchecked. A form of error mitigation called zero noise extrapolation (ZNE) can decrease an algorithm's sensitivity to these errors without increasing the number of required qubits. Here, we explore different methods for integrating this error mitigation technique into the Variational Quantum Eigensolver (VQE) algorithm for calculating the ground state of the HeH^+ molecule at 0.8Å in the presence of realistic noise. Using the Quantum Scientific Computing Open User Testbed (QSCOUT) trapped-ion device, we test three methods of scaling noise for extrapolation: time-stretching the two-qubit gates, scaling the sideband amplitude parameter, and inserting two-qubit gate identity operations into the ansatz circuit. We find time-stretching and sideband amplitude scaling fail to scale the noise on our particular hardware in a way that can be directly extrapolated to zero noise. Scaling our noise with global gate identity insertions and extrapolating after variational optimization, we achieve an estimate of the ground state energy within -0.004 ± 0.04 Hartree; outside chemical accuracy, but greatly improved over our non-error-mitigated estimate with error 0.127 ± 0.008 Hartree. Our results show that the efficacy of this error mitigation technique depends on choosing the correct implementation for a given device architecture.

I. INTRODUCTION

Quantum computers offer the promise of speedup over classical computation for several problems, including factoring and quantum simulation [1, 2]. One application of quantum simulation that has been extensively studied is in the field of quantum chemistry [3, 4], particularly the application of finding the ground state energy of a molecule [5]. A full-configuration interaction (FCI) approach to this requires storing the molecule's full electronic wavefunction, which has a dimension that scales exponentially with the number of electrons in the molecule. However, in a quantum computer the number of qubits required to represent this problem grows polynomially with the number of particles rather than exponentially.

Advances in quantum hardware have brought us into the so-called Noisy Intermediate Scale Quantum (NISQ) era [6]. NISQ machines today are characterized by a number of qubits ranging from 50 to a few hundred, and are notable because machines of this size begin to eclipse what is considered possible to simulate on existing supercomputers [7–10]. However, NISQ devices lack error correction, with two-qubit error rates around 0.1% [10–14]. Such errors can dramatically impact the performance of NISQ algorithms if left unchecked, as they can propagate and compound throughout a circuit's run-time.

Because of this, there has been a great deal of recent work developing, studying, and applying error mitigation methods to NISQ devices, as summarized in [15]. These techniques can improve the accuracy and precision of NISQ algorithms without requiring the large infrastructure needed for fault-tolerant quantum comput-

ing. In particular, zero-noise extrapolation (ZNE) stands as a method that does not require any qubit overhead, merely requiring precise control of the hardware and increasing the number of expectation values that must be measured. ZNE can reduce the bias of an expectation value at the cost of measuring multiple expectation values, each in turn requiring a sufficient number of samples or circuit executions to build up enough statistics to reach the desired level of precision. Previous studies have shown that this technique can improve the accuracy of expectation values using superconducting qubits [14, 16, 17] and trapped ion qubits [18, 19].

Here, we focus on the hurdles of practically executing zero-noise extrapolation on a trapped ion device. We implement extrapolation using three different techniques: 1) Adjusting the duration and detuning of the entangling gates in our circuit while keeping the amplitude constant, 2) Adjusting the detuning and amplitude of the entangling gates while keeping the duration constant, and 3) Inserting entangling gate identity operations. We study these techniques in the context of the Variational Quantum Eigensolver (VQE) algorithm [20, 21], which is suited for NISQ architectures. Our experimental results are obtained using the Quantum Scientific Computing Open User Testbed (QSCOUT), a trapped-ion qubit system based on Ytterbium ($^{171}\text{Yb}^+$) ions [11]. We investigate how to best implement this technique on our particular hardware, for our specific optimization procedure, given a fixed sampling budget.

In the remainder of Section I, we introduce the device and algorithm. In Section II, we discuss our noise model and how we chose to scale the noise present in our simulations and experiments. Section III shows the details of

our optimization routine, as well as our tests and results from simulation of our noise scaling methods. Section IV presents our results from running extrapolation experiments on the hardware. We finish with a discussion in Section V.

A. Device Details

This set of experiments was performed on QSCOUT’s room temperature system, a trapped ion quantum computer that exploits the hyperfine ‘clock’ states of $^{171}\text{Yb}^+$ ions ($^2\text{S}_{1/2}$ $|F=0, m_F = 0\rangle$ ($|0\rangle$) and $|F=1, m_F = 0\rangle$ ($|1\rangle$)). The ions are arranged in a linear chain and have all-to-all connectivity through their vibrational modes.

Parameterized single and two-qubit gates on this system are generated via Raman transitions using a pulsed 355 nm laser. The pulsed laser is split and delivered to the ions in a counter-propagating configuration, where on one of the arms, a single-channel acousto-optic modulator (AOM) is used to generate a global beam that covers all the ions, and a multichannel L3Harris AOM on another arm is used to generate a set of individual addressing beams that are each focused on individual ions. Using the experiment hardware ‘Octet’, two frequency tones can be applied to each channel of the AOMs.

For these experiments, we only require a simple, limited gate set (FIG. 1). To perform the single-qubit X gate, two Raman tones are applied to single individual addressing beams. The $R_z(\theta)$ gate is virtual and acts as a phase shift on all subsequent waveforms for that particular qubit. To perform the two-qubit Mølmer-Sørensen (MS) gate, two tones are applied to the individual addressing beams targeting the ions in the gate while another tone is applied to the global beam, thereby generating Raman transitions that have been symmetrically detuned from red and blue sidebands. In our system, this is equivalent to an ‘ XX ’ interaction. The inverse gate (MS^\dagger) is performed by shifting the phase of the waveforms applied to the second ion in the gate by π radians, converting the gate to an ‘ $-XX$ ’ interaction.

B. Zero Noise Extrapolation

Zero noise extrapolation (ZNE) is an error mitigation technique used to improve the accuracy of expectation values when given access to more measurements [16, 22]. Rather than attempting to lower error rates, which requires improvements to hardware, the error in the quantum circuit is instead deliberately and controllably increased. The thought is that if the amount of noise added to the circuit can be carefully scaled by some multiplicative *scale factor* c , then multiple noisy expectation values can be measured at set noise intervals. A function can then be fit to this data and traced backwards to obtain an improved, noiseless estimate for the expectation value at $c = 0$. Numerous techniques have been attempted in the

past to scale the noise in quantum circuits [16–18, 22, 23], some of which will be touched on in Section II.

Zero noise extrapolation comes at the cost of increased sampling overhead. For each noiseless estimate, m noisy estimates must be made, each needing samples to meet a desired precision. The variance in the noiseless estimate necessarily depends upon the variance of each of the noisy estimates, but it also depends on the kind of extrapolation used. In the simplest case, a linear function is fit to the data using least-squares regression or something similar. We generally expect that for most noise models, there is a direct relationship between the amount of noise added to the circuit and the energy difference between the noisy estimate and the ideal theoretical value. As such, a linear extrapolation is a good starting point for most noise scaling techniques.

If the underlying theory of how the noise scales supports it, a higher degree polynomial could be fit to the noisy estimates instead. A special case, known as Richardson Extrapolation [24], occurs when the highest possible degree polynomial for a given number of data points is fit (polynomial of degree $m - 1$ for m data points). Higher degree polynomials double down on the trade-off inherent to extrapolation, further reducing the bias of our estimate but increasing the variance [23]. In the case of Richardson extrapolation, the number of samples required to keep the variance constant scales exponentially with m , the number of noisy estimates. As such, if the noise trend is imprecise, it is less useful to fit higher order polynomials. This turns out to be true in this work, as discussed more in Section IV. In the case of a purely depolarizing noise model, the data may be best fit by an exponential decay [22].

Another important consideration is how many noisy estimates are measured for extrapolation. The fewer data points that are used, the more ‘overfit’ the extrapolation will be, with the fitted curve closely following the data. This is good if the noise scaling is very precise, as the resulting noiseless estimate will have high accuracy and precision. However, if there are fluctuations in the values of noisy estimates that are not directly derived from the noise scaling, or if the noise scaling only increases a portion of the noise present in the device, then fitting to fewer data points will result in more bias. On the other hand, increasing the number of noisy estimates not only requires more samples to maintain the desired precision, but also requires that the noise scaling technique allow for that many different noise values to be implemented on the hardware. For the number of samples we have access to on the hardware, we settle upon using a linear or quadratic extrapolation using 4–5 noisy energy estimates fit using weighted least-squares regression. This offers a balance of not over-fitting our extrapolation without ballooning the required number of samples.

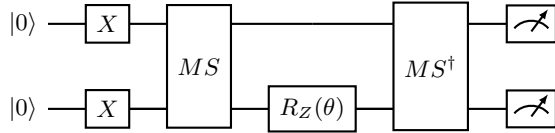


FIG. 1. The UCCSD ansatz circuit for HeH^+ in the STO-3G basis. The circuit structure remains unchanged across different bond lengths, with only the value of the optimization parameter θ varying.

C. VQE Algorithm and Ansatz

We use zero noise extrapolation to find the ground state energy of the small diatomic molecule HeH^+ using VQE as in [25]. We first encode the electronic Hamiltonian of the molecule to act on qubits using a python package, OpenFermion [26]. We can reduce the size of the HeH^+ encoding to 2 qubits in the manner shown in [27]. For our ansatz, we implement the Unitary Coupled Cluster for Singles and Doubles ansatz (UCCSD) [28–31] comprised of MS gates and a parameterized Z -rotation by a variational parameter θ as shown in FIG. 1 [27, 32]. The resulting circuits are then performed on QSCOUT.

For our classical optimizer, we chose to use the Constrained Optimization by Linear Approximation (COBYLA) gradient descent search algorithm as a part of the SciPy optimize package [33, 34]. For a problem of this scale with a single optimization parameter, this algorithm converges quickly and accurately to the ground state, even in the presence of noise. It is important that the classical optimizer be able to efficiently find the ground state in the presence of sampling noise, so that more of the total sampling budget can be allocated to performing the extrapolation procedure that follows.

This small quantum chemistry problem serves as a good test for exploring how error mitigation techniques such as ZNE can best be integrated into a VQE optimization routine. The simplicity of the ansatz circuit allows us to implement varied methods of noise scaling without the state decohering too quickly. To test these methods, we will first need to understand the noise in our device and how to controllably scale it.

II. NOISE MODEL IN SIMULATION

In order to increase the noise in our device, we need to pinpoint what kinds of noise are most likely to occur. Current NISQ devices are prone to a variety of sources of noise, and our extrapolation needs to take all such sources into account to scale the noise systematically. An extrapolation routine which only takes into account some noise in the device can still show improvement, but any unscaled noise source will affect the accuracy of the extrapolated result. The following section details how different

kinds of errors can be amplified by different noise scaling methods.

In simulation, the noise in our circuits is implemented using the internal software package at Sandia National Labs called “IonSim” that emulates the experimental control errors outlined in the original QSCOUT engineering paper [11]. IonSim takes in parameters such as the laser-pulse amplitude, frequency, phase, and duration. From the values of these inputs, IonSim then simulates each gate by solving the Master equation and generates process matrices that contain the physical errors. The result is a physically-motivated model meant to represent the QSCOUT device when subject to typical amounts of experimental noise, including drifts in the control parameters that can occur between calibrations.

Throughout this paper, we model single-qubit rotations about the z -axis on the Bloch sphere as ideal gates since these are implemented virtually through phase updates on the hardware, and we simulate all other single-qubit gates, $R(\phi, \theta)$, using a square pulse with gate duration of $(\theta/\pi) \times 22.8 \mu\text{s}$, where ϕ and θ are the rotation axis and the rotation angle on the Bloch sphere, respectively. In contrast, we use two different MS -gate implementations in this paper: one for the time-stretched noise scaling that we will describe in section II A and a separate one for the discrete noise scaling that we will describe in section II C.

For both MS -gate implementations, we use a time-dependent Rabi rate for the carrier transition of both ions, $\Omega(t)$, with a Gaussian pulse shape. This pulse has a duration of τ , is peaked about $t = \tau/2$, has a standard deviation of z , and has a peak Rabi rate of Ω_0 . We primarily target the tilt motional mode of the ion chain in one of the two orthogonal radial directions with a motional frequency of 1.75 MHz, and we apply two Raman laser tones detuned by $\delta_b = \delta$ and $\delta_r = -\delta$ from the blue and red sidebands of this mode, respectively.

For the discrete-noise-scaling implementation, we choose $\tau = 300 \mu\text{s}$, $z = 39.8 \mu\text{s}$, $\delta = -19.6 \text{ kHz}$, and $\Omega_0 = 80.2 \text{ kHz}$. For the time-stretched MS gates, we implement different gates based on the value of a noise-scaling parameter, c_τ , which linearly stretches the gate duration: $\tau = c_\tau \tau_1$. To target the same gate for different values of c_τ , we fix the peak Rabi rate at $\Omega_0 = 107 \text{ kHz}$ and linearly scale the other gate parameters: $z = c_\tau z_1$ and $\delta = c_\tau \delta_1$. For these gates, we choose $\tau_1 = 200 \mu\text{s}$, $z_1 = 26.5 \mu\text{s}$, and $\delta_1 = -34.5 \text{ kHz}$.

For all of these MS -gate simulations, the ions traverse a loop in phase space that corresponds to an ‘ XX ’ interaction, achieving an MS gate with $\phi = 0$ and $\theta = \pi/2$. To simulate an inverse MS gate, we perform similar simulations but introduce an ion-dependent phase shift of π to produce a ‘ $-XX$ ’ interaction and achieve an MS gate with $\phi = \pi$ and $\theta = -\pi/2$, which we define as MS^\dagger .

We then construct the IonSim noise model by introducing errors into the R and MS gate simulations. These errors are informed by characterization experiments that measure typical amounts of drift between calibrations

and result in typical gate fidelities. For both the R and MS gates, we introduce an absolute power offset that increases the Rabi rate by 5% of its peak value at all times. With this error only, the simulated $R(\phi, \theta = \pi/2)$ and $R(\phi, \pi)$ gates have a fidelity of 99.8% and 99.4%, respectively. For the MS gate, we also introduce a 500 Hz error in the motional frequency, give the ion a temperature of 0.5 q at the start of each gate, and introduce a 600 q/s heating rate during each gate. While the heating rate of the tilt mode is much smaller than 600 q/s, this rate represents the effect of the 1.6 kq/s heating rate on the much further detuned center-of-mass mode that we have otherwise neglected from the simulations yet dominates the fidelity impact from heating. With these errors, simulations of our discrete-noise-scaling implementation of MS gates produce an entanglement fidelity of 98.5% for both the MS gate and its inverse, separately, and an entanglement fidelity of 98.1% for the MS gate followed by its inverse. In our simulations throughout this paper, we apply these same gate descriptions to each appearance of a gate in a quantum circuit, neglecting all potential non-Markovian effects including additional drifts, fluctuations, and context-dependent errors.

A. Time-Stretched Noise Scaling

In general, the strength of the noise in a quantum circuit is not easily controllable through experimental means, as that would require a highly detailed noise model of the device. By definition, noise arises because of effects in the system that are not understood in detail. However, as was first shown in [17], this obstacle can be circumvented if we assume the noise in the circuit is time-translation invariant. For solid-state qubits, such as superconducting devices where qubits rest on top of a substrate and are constantly interacting with their environment, this assumption generally holds. The environment acts as a static source of error over the duration of the gates. For other architectures such as photonic systems, there may be no such source of time-translation invariant noise, with the vast majority of noise coming from control errors in the implementation of quantum gates. We believe that ion-trap devices fall somewhere in the middle, having some sources of time-translation invariant noise, and some sources of other noise.

As in [17], we first implemented ZNE by scaling the time it takes for our circuit to run. Assuming the noise is time-translation invariant, the noisy expectation value of the circuit will be the same if we run it with noise λ for a scaled time $c_i\tau$ as it would be for scaled noise $c_i\lambda$ for a time τ . We can make noisy estimates of the energy by lengthening the duration of gates in our circuit, rather than scaling the noise directly. We implement this in the hardware by keeping the amplitude of the control pulse constant while increasing the duration of the pulse and increasing the detuning of the motional sidebands. We will refer to this method as time-stretching the gates.

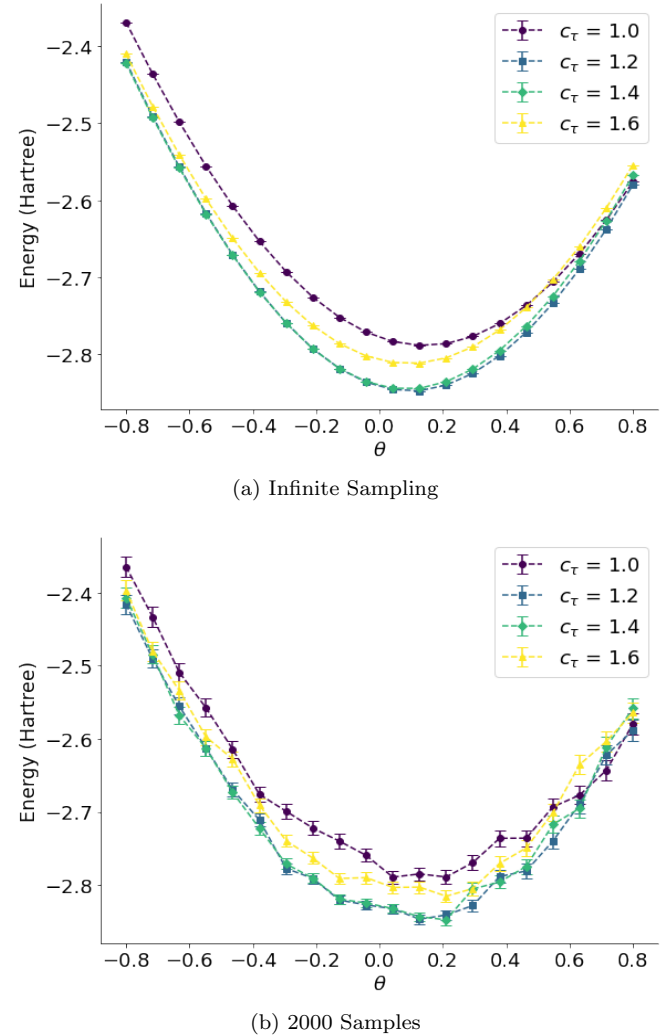


FIG. 2. **Simulation** — Comparison of time-stretched extrapolation with and without sampling noise. Curves are shown in color, labeled with a stretched duration relative to an unstretched circuit of duration τ (purple circles). (a) Even with infinite samples, the simulated noisy energy curves show some overlap and exhibit non-linear scaling. (b) With 2000 samples for each Pauli term in the Hamiltonian, the noisy energy curves have significant overlap, leading to poor extrapolated estimates.

In the case of time-stretched gates, we include a time-stretch factor c_τ indexed from $i = 1, 2, \dots, m$ that scales the gate duration by a multiplicative factor between 0.6 and 1.6, where $\tau' = \tau c_i$ and i indexes each noisy estimate. In order to achieve ideal MS gate performance in the noise-free model, both the Rabi rate Ω and the detuning δ need to be scaled by c_i as well, where $\Omega' = \Omega/c_i$ and $\delta' = \delta/c_i$. Although the time-stretch factor does not modify the magnitude of the physical errors in the IonSim noise model, this factor increases the sensitivity of the gate performance to errors due to the side effects it has on the Rabi rate and detuning.

In simulation, we find that the noise scales non-linearly,

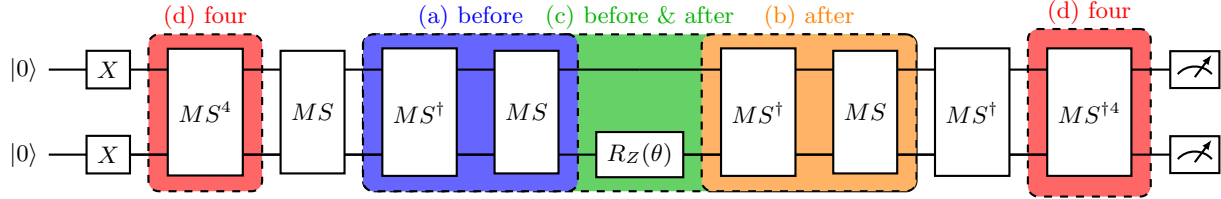


FIG. 3. The UCCSD ansatz circuit for HeH^+ shown in FIG. 1 with possible gate identity insertions. $(MS^\dagger MS)^i$ can be inserted before the parameterized $R_z(\theta)$ gate (a) blue, after (b) orange, or both (c) green. $(MS)^{4i}$ and $(MS^\dagger)^{4i}$ can also be inserted in both halves of the circuit (d) red.

as shown in FIG. 2a. We find that as we increase the duration and the detuning, the noise first decreases, and then increases as the circuit is lengthened. This does not bode well for extrapolation, as we would expect a direct relationship between the duration and amount of noise. A second potential problem with this method of extrapolation is the magnitude of the variation in the noise. Only a small amount of variation in the energy is introduced by time-stretching our circuits, on the order of $\sim 1 - 2\%$ of the unstretched circuit's energy estimate, meaning that the noisy estimates are tightly clustered together. This is in contrast with previous results from [17], wherein noise scaling is on the order of $\sim 1 - 10\%$. As seen in FIG. 2b, when each energy estimation is made with a fixed sampling budget of 2000 samples, the sampling noise may cause the noisy estimations to further overlap, rendering extrapolation ineffective. To solve this issue of resolution, we might try to increase the noise scaling of our circuits from 2 up to 5 or even 10 to better space out the noisy energy curves. However, increasing the duration of the circuit in this way directly scales the runtime as well. In order to get noise scaling of a magnitude amenable to extrapolation, we would need to increase the duration by at least a factor of 10. But, if we scale the noise too much, then the resulting decoherence may cause the noise scaling to become even more nonlinear, or worse render the action of our ansatz circuit useless. This is further explored in Section IV A. From these results, we expect this method of increasing the noise by stretching the duration of gates to be insufficient for successful extrapolation, as it does not scale the noise enough to be useful.

B. Motional Mode Detuning Scaling

A possible explanation for the previous time-stretching results is that pulse duration is not the gate parameter that we should be changing to scale the noise, but that we should be changing the detuning instead. For the previous method, the pulse amplitude was held constant, and the pulse duration was directly varied. In order to ensure that the MS gate performs the correct operation at longer duration, a third parameter called the sideband amplitude was re-calibrated and increased. We consider now if this parameter is the source of the noise scaling seen in FIG. 2.

By decreasing the power applied to these sidebands, we could recalibrate the system to a smaller detuning and determine how much noise is added in this process by measuring the relative infidelity of our two-qubit gates as we change the detuning parameter. For each value of the detuning parameter we want to use, we may calibrate the pulse duration and amplitude for ideal gate operation. The fidelity of that gate can then be approximated by stacking two gates and contrasting the population of the $|00\rangle$ state under a rotated frame before and after. In practice, we find that there is a range for the detuning parameter that yields the best results, between -15kHz and -7.5kHz. For larger detunings outside this range, the gate fidelity asymptotes the experimental ideal of $\sim 98.5\%$. On the other side of this range, the gate fidelity falters and approaches a fully decohered quantum state at ~ 0.50 . Thus, we set our baseline noise to be $c_1 = 1.0$ for the -15kHz gate, as this is where gate performance begins to noticeably suffer. Subsequent noise scalings are calculated as:

$$c_i = \frac{1 - F_i}{1 - F_1}, \quad i = 1, 2, \dots, m \quad (1)$$

where F_i is the measured fidelity of the gate for the i^{th} detuning parameter. Because of the small infidelity for the first parameter ($\sim 1.5\%$) the noise scalings for this method are much larger than those used for the other noise scaling methods, running as large as $c_i \sim 25$. The experimental extrapolation results for this technique can be found in Section IV B.

C. Gate Insertion

An alternative manner of scaling control errors in our circuits is to make discrete changes at the circuit-level, rather than changing the duration of the gates themselves, as described in [23, 35, 36]. Gate-insertion methods scale the noise in the circuit by varying the depth of the circuit rather than gate duration. A gate may be replaced by a series of gates:

$$U \rightarrow U(U^\dagger U)^i \quad (2)$$

where $i = 1, 2, \dots, m$ is a positive integer that indexes how many insertions have been made. By inserting the identity $U^\dagger U$ this way, the logical structure of the circuit is

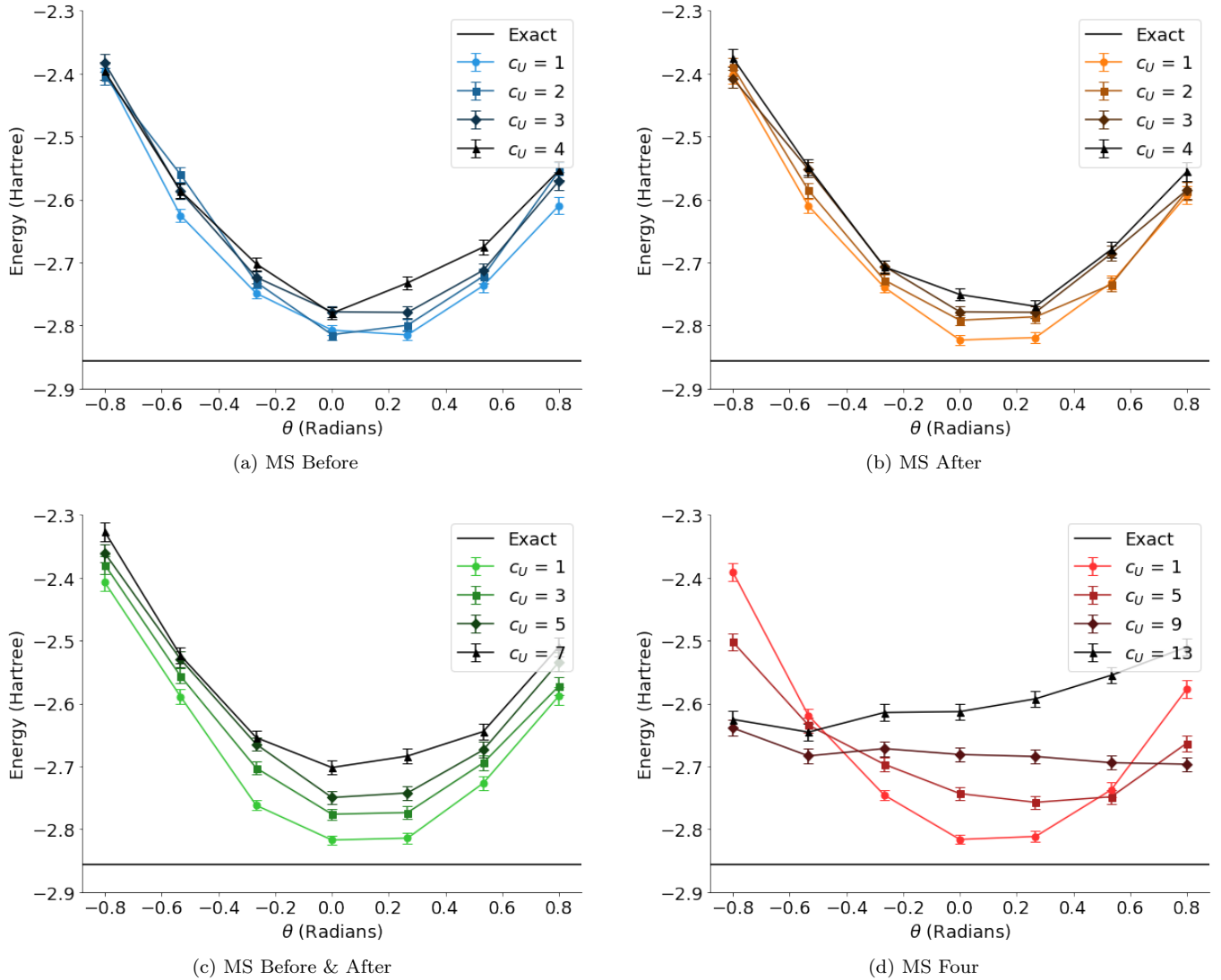


FIG. 4. **Simulation** — Comparison of different gate-insertion methods for $m = 4$ different scale factors c_U . All methods use 2000 samples per projective measurement. (a) *MS Before* - Inserting $(MS^\dagger MS)^i$ into the first half of the circuit. (b) *MS After* - Inserting $(MS^\dagger MS)^i$ into the second half of the circuit. As expected, we find that methods a and b are similar, since they both add the same number of gates to the circuit. (c) *MS Before & After* - Inserting $(MS^\dagger MS)^i$ into both halves of the circuit. Method c can be thought of as the sum of methods a and b, and the data shows this, as it has increased scaling. (d) *MS Four* - Inserting $(MS)^{4i}$ and $(MS^\dagger)^{4i}$ into the both halves of the circuit. Method d scales the noise differently, as shown by the altered shape of the energy curves. The noisy energies at the minimum parameter show consistent scaling, but the shape of the energy landscape changes with scale factor.

maintained while the effects of the noise are scaled by a factor c_U .

This technique can be applied to the entire circuit all at once in a process called *global folding* [23] to get an integer scale factor depending on the number of identity insertions. As we are interested in amplifying the noise due to our *MS* gates, we limit our insertions to those gates alone using *local folding*:

$$MS \rightarrow MS(MS^\dagger MS)^i \quad (3)$$

This has the effect of amplifying control errors in our

gates in a controlled manner. We tested this identity insertion before and/or after the parameterized $R_z(\theta)$ gate in the ansatz circuit. We note, however, that this method may fail to scale certain kinds of coherent errors in the circuit. Because we are inserting a gate followed by its inverse, it is possible that some errors introduced will be immediately cancelled out rather than increased. If the majority of the noise in the circuit is due to coherent errors that cancel in this way [37], then this method will add little to no noise to the circuit. This would render extrapolation futile, as our goal is to amplify all the errors

incurred in the unstretched circuit.

A possible workaround to this cancellation is to instead scale the noise by inserting a different set of gates, so long as those gates also comprise an identity operation. For instance, we may choose to instead scale our MS gates as follows:

$$MS \rightarrow MS(MS)^{4i} \quad MS^\dagger \rightarrow MS^\dagger(MS^\dagger)^{4i} \quad (4)$$

where we now insert the identity in the form of four Mølmer-Sørensen gates each with $\phi = 0$, $\theta = \frac{\pi}{2}$, the same parameters as our usual MS gate. This kind of discrete gate insertion would circumvent cancellation of certain coherent errors, as we never follow up an entangling operation with its inverse. However, this method requires that four two-qubit gates be inserted at a time for each preexisting two-qubit gate in our circuit, which introduces a lot of noise very quickly. This low resolution in the amount of noise that we are able to add to the circuit as a function of the number of insertions may make it difficult to perform extrapolation. We want to have enough distinct noisy energy estimates (and thus enough insertions) to ensure that our extrapolation does not over-fit our data, but as we add more and more gates to our circuit we run the risk of decoherence overshadowing all other forms of noise, negating the effect of our ansatz circuit.

We expect all of these methods to generally scale the noise in our circuit as a function of the total number of two-qubit gates. The unstretched ansatz circuit contains two MS gates, so the scale factor for a given noisy circuit can be written as the ratio of the number of two-qubit gates in the noisy circuit over two. Different noise scaling methods add a different number of two-qubit gates with each insertion, but the general formula for the noise scaling can be written as:

$$c_U(i) = \left(\frac{X}{2} * i \right), \quad i = 1, 2, \dots, m \quad (5)$$

where i indexes how many identity operations have been added to the circuit starting with no insertions for the unaltered circuit with $c_U(1)$, and X is how many two-qubit gates have been added with each identity. For the MS *Before* or MS *After* methods, wherein two gates are added, this corresponds to a scaling of $X = 2$ with scale factors $c_U = 1.0, 2.0, 3.0, \dots$. The MS *Before and After* method adds four gates with each iteration, corresponding to a scaling of $X = 4$ and scale factors $c_U = 1.0, 3.0, 5.0, \dots$. Lastly, the MS *Four* method adds eight two-qubit gates with each iteration, corresponding to a scaling of $X = 8$ and scale factors $c_U = 1.0, 5.0, 9.0, \dots$. These trends are all linear, and represent our best guess for how much noise will be added to the circuit as a function of the number of gate insertions.

We show these different identity insertions in FIG. 3 and compare their effectiveness in simulation in FIG. 4. We plot noisy energy curves for different scale factors as in Section II A, varying θ between -0.8 and 0.8 . Here, we

use 2000 samples per estimate of the expectation value of each term in the Hamiltonian. This choice is in line with the number of samples we used in our later experiments in Section IV.

The results broadly show the expected behavior for these four methods, and the noise scaling is improved compared to FIG 2b. FIGs. 4a and 4b both show similar amounts of noise scaling, as they both insert the same number of two-qubit gates into the circuit. The noise scaling is around $\sim 3\%$ of the unstretched circuit's minimum energy, which is more in line with the results from [17], but still low. The only difference between the two is where those gates are added, but the symmetry of the ansatz means that choice does not have an effect on the overall error. They maintain the parabolic shape of the energy landscape, and do not significantly shift the location of the minimum. The noise scaling shown in FIG. 4c is in line with what we would expect from the summation of FIGs. 4a and 4b, sharing the same overall shape with more space in-between the energy curves. Here the noise scaling is around $\sim 5\%$, with the noisy energy curves overlapping less.

The energy curves in FIG. 4d are of a different shape, with significantly higher noise scaling. The $c = 9.0$ curve in particular shows flattening we would normally expect from a state that has been greatly decohered, with overall noise scaling on the order of $\sim 7\%$. Interestingly, when we add yet more gates to the circuit, the $c = 13.0$ curve regains its parabolic structure. If we study the full energy landscape from $\theta = [-\pi, +\pi]$ and compare, we find that the behavior of the two noisiest energy curves is an artifact of zooming in on this particular region of θ . Our noise model includes a $\sim 5\%$ over-rotation error in the angles of our MS gates, which is dramatically amplified by this noise scaling method. This is good, insofar as we are capturing that kind of noise in our scaled circuit, but this coherent error in the noise model also has the effect of changing the location of the minimum energy. This is in contrast with what we see in experiment, as shown later in FIG. 9d, where we see more stochastic error and less coherent error.

In addition to the challenges posed by coherent errors, a second difficulty in using gate identity insertions over the time-stretch method is determining the precise scaling of the noise in our circuit as a function of the number of gate insertions. If we assume that all gates contribute noise, then the noise would in turn scale proportional to the total number of gates. However, as we find that the majority of the noise in our experiments come from our two-qubit gates, we only consider the effect of those gates here. The scale factor of the noise added to the circuit is given by the ratio of the number of two-qubit gates in the altered circuit over the number of two-qubit gates in the base circuit, as described previously. For all the techniques outlined above, we find that this relationship holds true in simulation. As such, we choose our extrapolation coefficients in this manner going forward in Section IV.

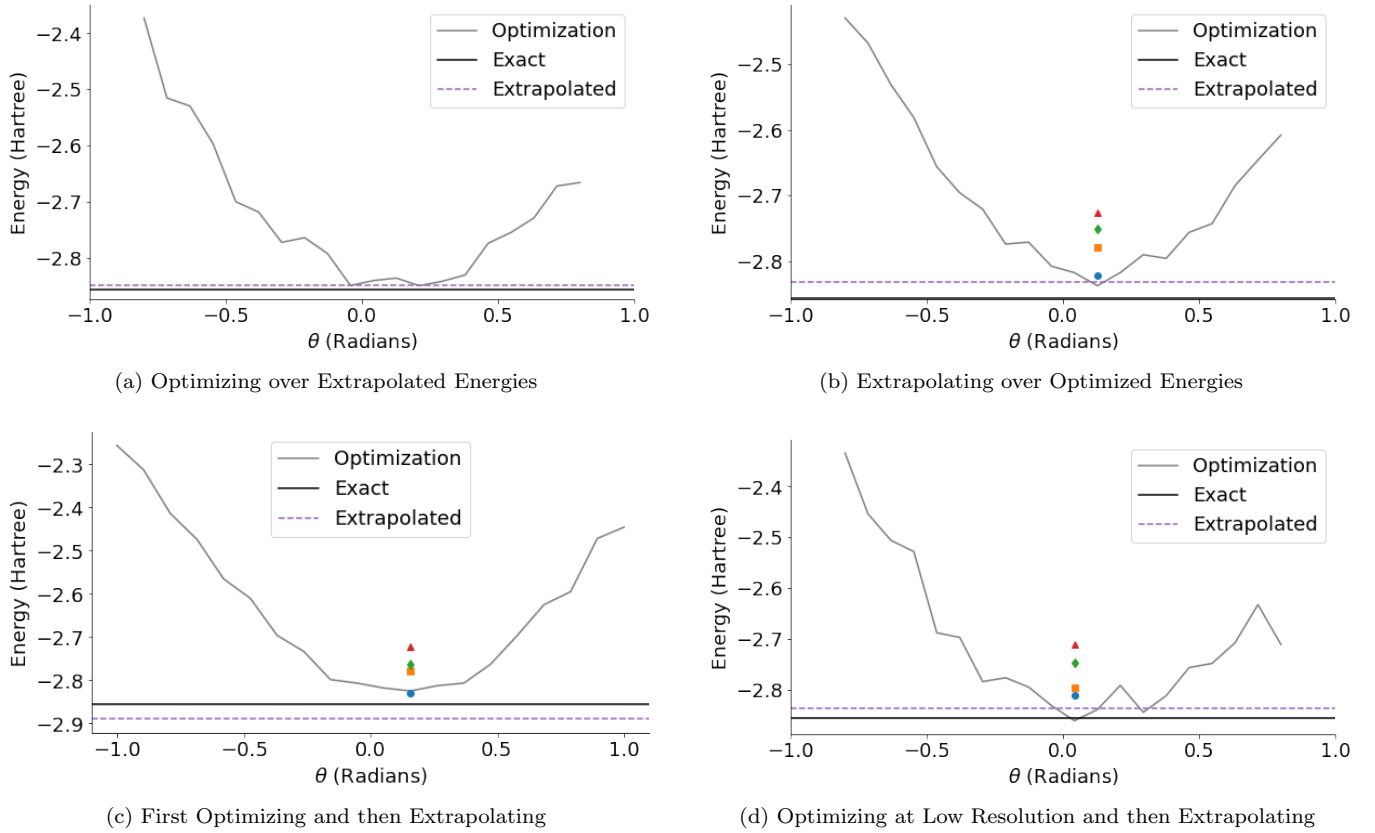


FIG. 5. **Simulation** — Comparison of four different methods to combine extrapolation and optimization. The single ansatz parameter is divided up into 20 values, with each routine utilizing the same total budget of $s = 28,000$ samples. The exact ground state is shown as a horizontal black line, and the extrapolated noiseless energy estimate as a dashed purple line. (a) Extrapolate m energies at each optimization iteration. (b) Optimize m separate energy curves and extrapolate from m minimum energies (here $m = 4$ highlighted points). (c) Find minimum without extrapolation and then use remaining sampling budget for final extrapolation. (d) Extrapolate with only two noisy energies at each optimization iteration to find minimum, and then extrapolate with four noisy energies for final extrapolation.

III. VQE SIMULATION WITH EXTRAPOLATION

Another aspect we explored was the relation between extrapolation and the classical optimization routine used in VQE. Extrapolation can increase the accuracy of expectation values measured on a noisy device, but it oftentimes does so at the expense of the precision of that estimate. As such, we wanted to know whether it is more efficient to incorporate extrapolation into the optimization routine, or if it is better to save extrapolation for the end of the algorithm to improve the final estimate. This section focuses on answering that question for our given problem using simulations.

A. Optimization and Extrapolation

As was outlined in Section IB, the accuracy and precision of extrapolation depends on both the number of noisy energy estimates measured and the number of sam-

ples used for said estimates. This sensitivity informs the design of our overall algorithm, as we wish to employ extrapolation and its large sampling cost only where it will show improved accuracy over unmitigated estimates. Multiple energy estimates are needed during a VQE optimization, and there are many ways to combine extrapolation and optimization. We now outline four such choices, as shown in FIG. 5.

(a) *Optimizing over extrapolated energies* involves preparing m scaled circuits and measuring m noisy expectation values for a single parameter θ at each step of the optimization. These estimates are then extrapolated to a single noiseless estimate, which is fed into our optimization routine alongside the parameter θ . This method is more algorithmically complex, as it requires us to perform our extrapolation numerous times in the middle of our optimization routine, costing us computational resources. We are no longer optimizing a physical quantum circuit, but rather a mathematical estimation of what we believe the noiseless circuit to be. We note that these extrapolated energies are no longer variational,

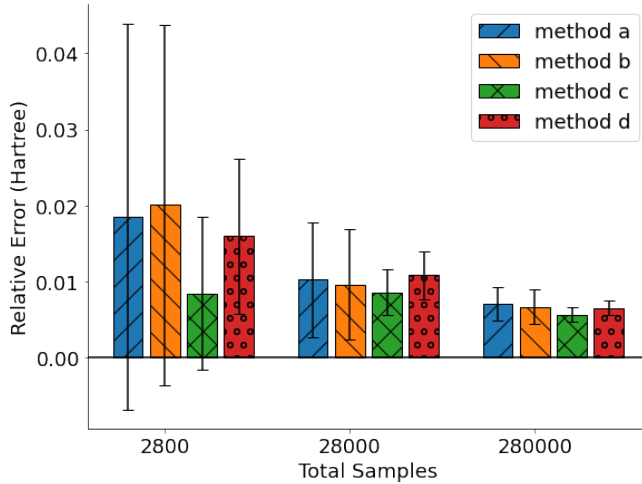


FIG. 6. Simulation — Comparison of the absolute relative accuracy and precision of four different optimization procedures as the total sampling budget is increased. Each method extrapolated the final noiseless energy estimate using a linear fit from $m = 4$ noisy energies using COBYLA optimization to find the optimal parameter θ . The results were averaged across ten trials. **(a)** Extrapolate from multiple noisy estimates at each step of the optimization routine. **(b)** Prepare multiple stretched circuits and optimize each of them separately before extrapolating using their respective minima. **(c)** Optimize an unstretched circuit to find a minimum and then extrapolate. **(d)** Extrapolate from only two noisy estimates at each step of the optimization, and then perform a high-resolution extrapolation at the minimum. Method c has the lowest variance across the varied number of samples and is the simplest to implement.

and therefore can dip below the exact ground state energy. This is a reasonable theoretical approach, however this method potentially exposes our optimization to the sampling sensitivities of higher-order extrapolation.

(b) Extrapolating over optimized energies is the inverse of *optimizing over extrapolated energies*. We prepare m stretched circuits and measure m noisy expectation values of the energy for m different parameters $\vec{\theta}$. We then do m independent optimizations in order to determine the minimum noisy energy for each scaled circuit. Once these minima are obtained, we then extrapolate the results to a single noiseless estimate as before. This method is simpler than the first, but poses its own problems. Firstly, it is still computationally intensive, as we must perform m full optimizations. Moreover, depending on how the circuits are scaled, the shape of the energy landscape of the corresponding Hamiltonian may change. This in turn may affect the minimum parameter θ for each of these scaled circuits. When we extrapolate the m distinct minimum energies, they may correspond to different locations on the energy landscape. We are in effect extrapolating the expectation values of different wavefunctions prepared with different parameters, potentially leading to a less accurate estimate.

(c) First optimizing and then extrapolating takes a similar approach to *extrapolating over optimized energies*, though it is further simplified. Instead of optimizing m distinct noisy energy curves, we can instead carry out the full optimization for a single, unscaled circuit as usual. If we assume that the energy landscape of this base circuit is relatively flat near the minimum, insofar as changes in θ have a smaller effect on the energy than the noise in our circuit, then this method should give a similar final optimization parameter as the noiseless circuit. We may then prepare m stretched circuits and measure m noisy expectation values of the energy for this final optimized θ and extrapolate the results to a single noiseless estimate. For a NISQ device like QSCOUT, where we have a finite budget of samples for a given experiment, this third method offers a balance between precision and cost. We find that for a small problem such as HeH^+ with only a single optimization parameter, an unstretched optimization does a good job of finding the minimum, as the energy landscape is a simple sinusoid. Therefore, we can focus our efforts on mitigating the noise present in the final energy estimate rather than spending resources improving the accuracy of our optimization.

(d) Optimizing at low resolution and then extrapolating builds on *first optimizing and then extrapolating* similar to [17]. If we wish to improve our initial optimization at the cost of more shots, then we can choose to perform our optimization with a low-resolution linear extrapolation procedure at each iteration using the minimum of two data points. This should give us a better noise-free estimate of the optimal variational parameter, and we can then perform a higher-resolution extrapolation using more data points at that parameter to obtain a more accurate final energy estimate. This method serves as a middle ground between methods (a) and (c).

We compare the accuracy and precision of these four algorithms in FIG. 6, averaged across ten trials. As expected, the extrapolated energies converge to the ground state energy as we increase the total sampling budget, with slight variations in the accuracy and precision between them. For experiments on the QSCOUT device, we are limited to $\sim 28,000$ total samples for the optimization before qubit-drift starts to become a problem, meaning we can expect relative errors on the order of 1%. We find that scaling the noise in the ansatz circuit does not have a large effect on the location of the minimum energy for all methods except for the *MS Four* method as seen in FIG. 4, and therefore we can get a good approximation of the optimal variational parameter by simply optimizing an unscaled circuit, as evidenced by the accuracy of method c. For a more complicated chemical system with a more complex energy landscape, we might have instead chosen to *optimize at low resolution and then extrapolate*, as doing so should mitigate errors incurred while measuring energies during the optimization procedure. We find that such a technique is unnecessary for HeH^+ .

For the rest of this work, we choose to optimize an

unscaled circuit and then extrapolate at the minimum parameter, corresponding to *first optimizing and then extrapolating* (method c). This choice requires the fewest samples from our total budget for the optimization procedure, meaning that those samples can be instead allocated to obtain precise noisy energy estimates at the optimal variational parameter. This precision will propagate through extrapolation and improve the accuracy and precision of our final noiseless energy estimate of the ground state.

IV. EXTRAPOLATION EXPERIMENTS

Having determined the method of scaling the noise in our circuit and the method of integrating extrapolation into the VQE optimization routine, we now turn to experiments on the hardware. The QSCOUT device requires frequent recalibration due to noise affecting the stability of the system. A full VQE optimization may take on the order of an hour to complete, depending on how many samples are taken. Over these timescales, the ions in the device can drift spatially out of the individual addressing beams, causing more gate errors. In particular, this kind of event leads to coherent under rotations of gates within circuits. In addition, fluctuations in the radio frequencies used to create the potential well to trap the ions can impact the device's performance. A large enough fluctuation can induce unwanted sideband transitions and interfere with the execution of gates. This error is not taken into account in our noise model, and as such the following results differ from the previous simulations.

Other sources of noise can be categorized as either stochastic or coherent. Stochastic errors include the qubits' interactions with their environment, such as an increase in the ion's motional states due to heating from the trap. There can also be stochastic amplitude fluctuations in the qubit control beams that randomly affect the implementation of gates. Coherent control errors include crosstalk between ions within the trap and static amplitude fluctuations in the qubit control beams. Most of these sources of noise are difficult to isolate and scale for extrapolation, as they can not be modeled as simple depolarizing noise.

We begin by time-stretching the duration of our gates, as it was the easiest to implement. In order to time-stretch the duration of the *MS* gates in our hardware experiments, we must increase the duration of the laser pulses used to implement said gates, which increased the symmetric detuning. Doing this and keeping all else the same, the same logical gate will be executed over a shorter or longer duration. We then test the effect of directly varying the sideband amplitude detuning parameter in our gates, keeping the duration constant and compensating with the pulse amplitude. Finally, we conclude with results from testing all four gate-insertion noise scaling methods. Throughout the rest of this section, we make our estimates using 2000 samples per projective

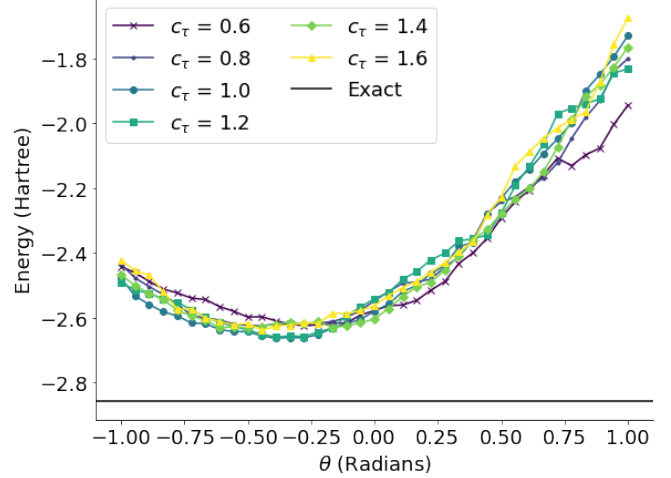


FIG. 7. **Hardware** — Experimental implementation of time-stretching gates with a finite sampling budget, similar to data shown in FIG 2b. Gate duration was varied between 0.6 and 1.6 times the typical operating duration of $\tau = 200\mu\text{s}$. 2000 samples were used to estimate each expectation value. The separation in energy curves for different scale factors are too small to differentiate with sampling noise and qubit drift.

measurement in the Hamiltonian.

A. Time Stretch Experiment

We began our experiments by testing the effectiveness of time-stretching via a sweep of the energy landscape. We measured our circuits, manually varying the optimization parameter θ from -1.0 to 1.0 in intervals of 0.05 . The result was a slice of the energy landscape for a given circuit timescale. We then repeated this process, changing the timescale of our *MS* gates between 0.6 and 1.6 times the standard scaling. The results of this test are shown in FIG. 7. We found that while the energy did depend on θ , there was little to no dependence on the scale factor. Lengthening and shortening circuits from normal operating pulse duration conditions did not increase the noise enough to differentiate the noisy energy estimates in the presence of fluctuations due to sampling error and qubit drift. As simulations suggests, we are not able to extrapolate to an accurate noiseless estimate. We also separately tested the effects of stretching the gates at extremely long duration, but found that the noise increased abruptly at around $c_\tau = 3$.

We believe that our hardware is robust within this region to this specific implementation of pulse duration scaling. It is possible that some other implementation of time-stretching would work, but we chose to shift our attention to other methods of scaling the noise going forward. Though a naive implementation of time-scaling circuits worked well in [38] where a superconducting qubit device was tested, the same appears not to hold true for trapped ion devices such as QSCOUT. In practice,

lengthening the timescale of our circuit did not change the amount of noise present in our algorithm at reasonable scale factors.

B. Sideband Amplitude Experiment

Next, we performed extrapolation with the sideband amplitude scaling method. We adjusted the power applied to the red and blue sidebands such that the necessary detunings for the gate were across a wide range, from -40kHz all the way down to -6kHz. To find each desired detuning, we calibrated the MS gate to specific powers applied to the sidebands and measured a noisy expectation values using 2000 samples per projective measurement. Within this range we found that changing the parameter only had an effect on the energy within the range of -15kHz to -7.5kHz, as described previously in Section II B and shown in FIG. 8a. These energies were plotted versus their corresponding noise scaling in FIG. 8b and fit using total least squares regression from SciPy.ODR [34]. This regression technique takes into account the y -error in the noisy energies themselves, as well as the x -error derived from our uncertainty of the gate fidelity for different values of the detuning parameter.

We compare the goodness of our fits by looking at two statistical metrics: reduced chi-squared and adjusted R-squared. Both are computed ‘ex post facto’. Reduced chi-squared is a squared ratio of how far away each data point is from the fit compared to the error bar of that point, also known as the residual sum-of-squares. Here, we take into account contributions in both x and y . We then divide this value by the number of degrees of freedom in the fit, or the number of data points minus the number of fit parameters. The reduced chi-squared values of these two extrapolations are both greater than one, on account of the small y -error bars relative to the difference between the data points and fits. We obtain values of 5.85 and 2.55 respectively for the linear and quadratic fits, indicating the quadratic fit is better. The adjusted R-squared values show a similar trend. R-squared is a measure of how much better a fit is compared to a flat weighted average of the data points. It is calculated by dividing the residual sum-of-squares by the total sum-of-squares, which is a similar measure comparing the difference between each data point and the weighted mean. R-squared is one minus this ratio, and adjusted R-squared additionally takes into account the number of degrees of freedom in the fit. Comparing the adjusted R-squared values of linear (0.987) and quadratic (0.993) fits to the data, we find that both fits are good on account of the large x error-bars, but a quadratic function best describes the relationship between the noise scaling and the noisy energies.

The energies follow a roughly linear trend as a function of the detuning parameter itself, but the fidelity (and therefore relative infidelity) of the gates follows a quadratic trend as a function of the detuning parameter.

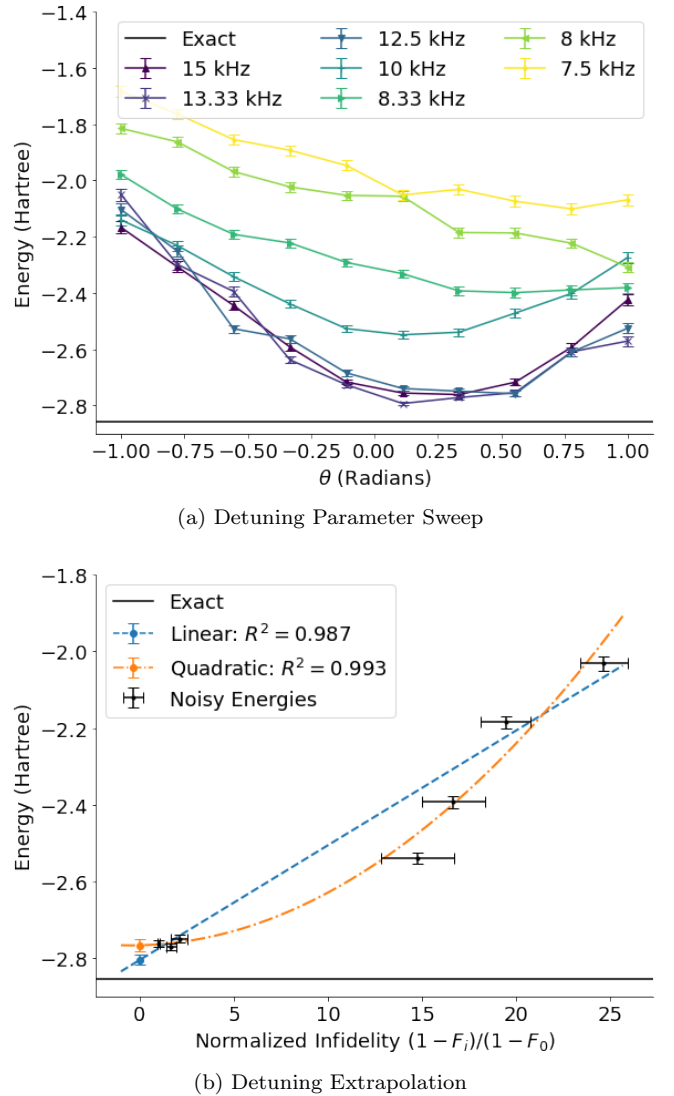


FIG. 8. **Hardware** — Experimental implementation of noise scaling by direct scaling of the sideband detuning parameter. (a) Noisy energy estimates were obtained for detunings: $[-15, -13.33, -12.5, -10, -8.33, -8, -7.5]$ kHz, using 2000 samples per projective measurement for different ansatz parameters θ . We see a degradation in the quality of the gate begin around -12.5kHz and level off around -7.5kHz, with a mostly linear regime in-between. (b) The data at the minimum variational parameter θ was fit using total least-squares to a linear function (blue, dashed) and quadratic function (orange, dot-dashed). The quadratic function best describes the data, leading to a noiseless energy estimate on par with the unaltered circuit. This energy gap implies that this method only scales a portion of the total noise present in the circuit.

Thus, the overall relationship is best fit by a quadratic function. This results in a noiseless energy estimate that is very close to that of the first noisy energy estimate, corresponding to the unaltered circuit. In other words, when we scale the noise using this technique, the energy trend approaches the unaltered circuit energy. We believe that this means that this method only scales a

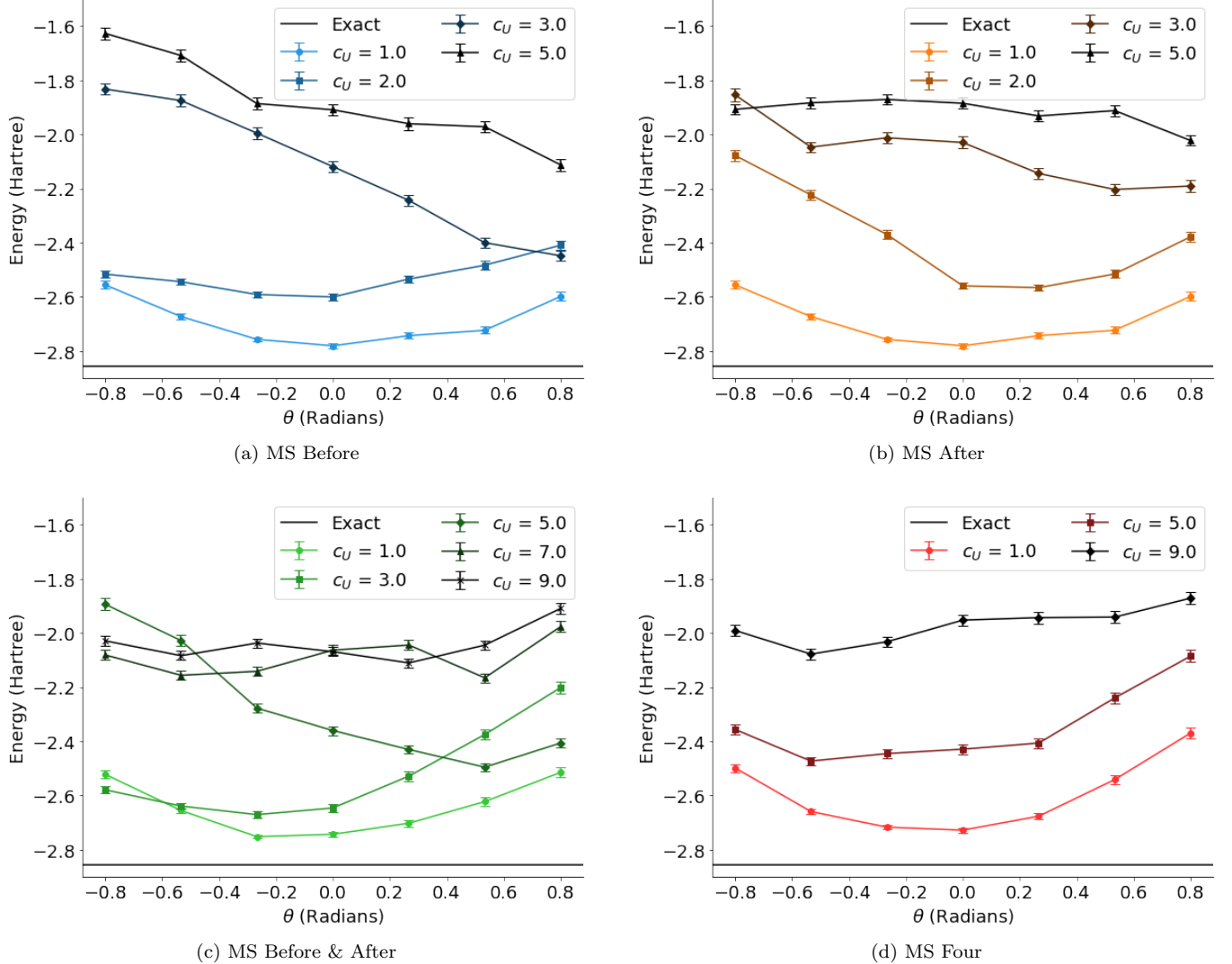


FIG. 9. **Hardware** — Comparison of gate-insertion methods implemented on the QSCOUT device. The data broadly matches the trends seen in FIG. 4. (a) Inserting $(MS^\dagger MS)^i$ into the first half of the circuit tractably scales the noise in the circuit, save for the outlier curve at $c_U = 3.0$. (b) Inserting $(MS^\dagger MS)^i$ into the second half of the circuit also tractably scales noise with similar results. (c) Inserting $(MS^\dagger MS)^i$ into both halves of the circuit scales noise at a similar rate to inserting into the first or second half. (d) Inserting $(MS)^{4i}$ into both halves of the circuit scales noise consistently, but not at the expected rate given by the scale factors.

small portion of the noise present in our ansatz circuit. As evidenced by the remaining energy gap, there exists a sizable amount of noise after extrapolation, which we believe is not being scaled using this technique, and thus not mitigated.

C. Gate Identity Insertion Experiment

Our subsequent experiments used discrete gate-insertion noise scaling methods. We repeated the same parameter sweep experiment as before, scaling the noise by inserting the identity operations described in Section II C. Each noisy curve is labelled with a scale factor c_U ,

indexed by $i = 1, 2, \dots, m$ and defined as the number of two qubit gates in the noisy circuit divided by the number of two qubit gates in the unstretched circuit. Between each trial, the sideband amplitude was recalibrated to correct for qubit drift. As the data shows in FIG. 9a, we find that the *MS Before* method injects much more noise in experiment than it did in simulation, as previously shown in FIG. 4a. The energies increase in accordance with the scale factor, though the curve corresponding to $c = 3.0$ seems to be an outlier, exhibiting more noise than expected at negative θ and less noise at positive θ . The data shown in FIG. 9b, wherein we use the *MS After* method, shows a similar, more consistent behavior. The noisy energy estimates using the *MS Before* &

After method in FIG. 9c are less consistent, particularly the $c = 5.0$ energy curve. Interestingly, we find that this experiment actually has less noise than either the *MS Before* or *MS After* methods. Lastly, the *MS Four* method adds more noise to the circuit with each iteration, but also scales the noise tractably, as the data in FIG. 9d shows. However, using this technique, we are limited to only three insertions before the energy plateaus due to decoherence.

We decided to further explore the *MS After* method for our following experiments, as the results from this experiment show similar trends to those found in simulation, as shown in FIG. 4. Though the energy curves in experiment fluctuate much more, as there are significant additional sources of noise not present in simulation, all the methods display enough of an energy gradient as we increase the noise scaling for some measure of extrapolation. In this case, the *MS After* method has the lowest variance across the $m = 4$ noisy energy curves. Moreover, we find this method works well following an optimization procedure. Using the same ansatz circuit and molecular parameters as in all other experiments, we performed a VQE optimization without any extrapolation. We used the COBYLA classical optimization algorithm [34] for our gradient descent, allocating 1000 samples per projective measurement for each iteration. The optimization converged to a minimum variational parameter after 21 steps.

We then performed extrapolation at that minimum parameter. Five noisy estimates were made, again using 2000 samples per projective measurement. These estimates fall in line with the final energy estimate from the optimization procedure, and we see a clear increase in the energy due to the noise scaling. These noisy measurements were then extrapolated to two noiseless estimates corresponding to a linear (blue dashed) and quadratic (orange dot-dashed) least-squares fit to the data, as seen in FIG. 10. We find that this extrapolation can improve the accuracy of the ground state estimate. The linear fit has an adjusted R-squared of 0.948 and a reduced chi-squared of 20, and the quadratic fit has an adjusted R-squared of 0.946 and a reduced chi-squared of 15. These values indicate that the two fits generally matches the data ($R^2 \sim 1$), but that the error bars are too small to explain the residuals seen in the noisy energies ($\chi^2 \gg 1$). Our error bars capture the sampling error within each data point, but do not account for coherent errors such as qubit drift due to heating between experiments that would shift the noisy energy estimates.

These residuals (relative to the theoretical linear noise scaling) are enough to significantly skew the fits for higher order polynomials. We attempted Richardson extrapolation (fitting a polynomial of degree $m - 1$ to m data points) using this dataset, but found it overfit the data, resulting in noiseless energy estimates far from the ground state energy. Even with only a quadratic fit, the noisy energy estimates at $c_U = 3.0, 5.0$ are higher than the expected linear noise scaling $c = 2i + 1$ outlined in

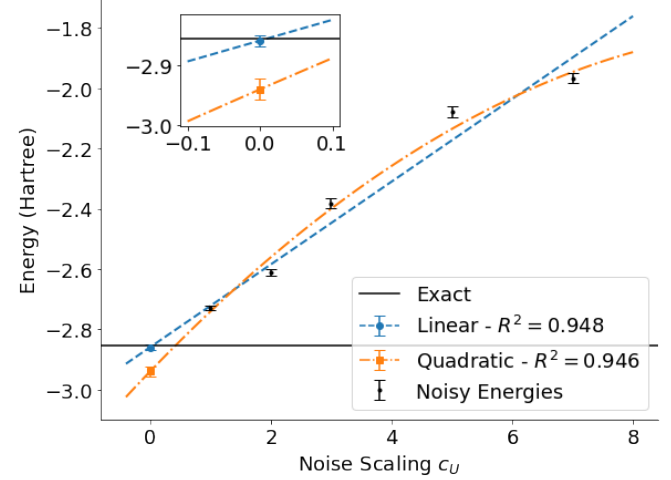


FIG. 10. **Hardware** — Extrapolated energies from measurements taken after optimization using the *MS After* method described in Section II C and the *first optimizing and then extrapolating* method described in Section III A. The noisy energy estimates are plotted as a function of the noise scale factor c_U . The black data points represent the $m = 5$ noisy energy estimates made at $c_U = 1.0, 2.0, 3.0, 5.0, 7.0$ that were used for extrapolation. The data was fit using a least-squares method to a linear (blue dashed) and quadratic (orange dot-dashed) function. The linear fit results in a noiseless energy estimate of -2.860 ± 0.040 Hartree, with relative error of only 3.2% compared to the unaltered circuit. The quadratic fit results in an energy of -2.940 ± 0.017 Hartree, with a relative error of 66% compared to the unaltered circuit.

Fit	Linear	Quadratic
Absolute Error	-0.004 ± 0.009	-0.085 ± 0.017
Relative Error	$0.143\% \pm 0.312\%$	$2.96\% \pm 0.610\%$
Error vs. No Extrapolation	3.2%	66%

TABLE I. **Hardware** — Results of gate identity insertion based extrapolation. We report the absolute accuracy and precision in Hartree, the relative error normalized to the ground state energy, as well as the comparative error of our extrapolated energy estimates vs. no extrapolation as a percentage.

Section II C, which shifts the quadratic noiseless estimate lower than the linear estimate. The linear estimate falls within error bounds of the ground state estimate, though it has a slightly larger reduced chi-squared value than the quadratic estimate. These results are summarized in TABLE I.

V. DISCUSSION

Our experiments show that there is a great deal of nuance when it comes to implementing zero noise extrapolation techniques on a trapped-ion NISQ device. Such methods are promising because they do not require more

qubits, however they are sensitive to sampling noise and necessitate a deeper understanding of the kinds of noise present in the system. A naive application of a given noise scaling method may not improve the accuracy or precision of an experiment by itself, due to the nature of the noise being a mismatch for the technique used.

We find that for our ion-trap system, QSCOUT, a time-stretching implementation of zero noise extrapolation does not scale the noise in the circuit enough to differentiate the resulting noisy energies in the presence of sampling noise. We contend this is due to the long coherence times of trapped ion qubits, such that they maintain the prepared state over the time scales of lengthened gate operations. This also shows that different noise mitigation techniques can be a probe of the types of noise present in a device. Additional experiments directly varying the detuning of the motional sidebands did a better job, but still failed to scale all the noise in the circuit. These experiments resulted in a quadratic trend and noiseless estimate with bias similar to no extrapolation.

By scaling the noise in our circuits using gate-insertion based methods, we find that zero noise extrapolation is possible on our trapped ion system, though improvements are only seen under certain circumstances. For our particular device, with the majority of noise coming from the implementation of our two qubit gates and an absence of too many coherent errors, gate-based noise scaling works best. With a budget of 2000 samples for each projective measurement, we were able to show an improvement using a gate insertion method wherein the MS gates in the second half of our ansatz circuit were scaled by repeated identity insertions of $(MS^\dagger MS)$. This method increased the noise in the ansatz circuit such that the resulting energy curves were distinguishable even in the presence of expected coherent errors. We found that there were still additional sources of noise in our experimental data, such as heating, that reduced the efficacy of extrapolation using higher order polynomials, though our linear fit obtained an improved noiseless energy estimate within -0.004 ± 0.04 Hartree of the ground state, a relative accuracy and precision of $0.142\% \pm 1.40\%$. Here we note that extrapolation is not variational, and therefore our estimate overshoots the ground state.

For optimization problems such as these with one variational parameter, we find that there is some flexibility in how one chooses to integrate extrapolation into the classical optimization of VQE. Choosing to extrapolate the data first before optimizing, or optimizing the data first before extrapolation does not have a large effect on the resulting error in simulation. These different techniques all obtain energy estimates within 2 – 5% of the true energy minimum for our fixed sampling budget, with the difference between them diminishing with more samples. What matters most for the optimization is how many samples are used for each projective measurement at each iteration. With this in mind, we choose to only optimize the unstretched ansatz circuit, as we believe

that the typical noise in the circuit does not meaningfully change the location of the optimal parameter for this problem. Limiting the optimization in this way allows us to allocate more samples to each iteration, improving the precision. Following this optimization, our extrapolated noiseless estimates for the expectation values of our UCCSD ansatz for HeH^+ lie closer to the true ground state energy. This improvement comes with a price: every noiseless energy estimate requires m multiple noisy energy estimates, and thus m times the number of samples for the same precision. If we were to allocate the same number of samples to the unscaled circuit, we would see improvements to the precision of our estimates, but no such improvement to the accuracy.

We achieve a noiseless energy estimate with an accuracy and precision of -0.004 ± 0.04 Hartree, within error bounds of the ground state energy of the HeH^+ molecule. These results are in line with previous VQE experiments. The original paper studying HeH^+ [20] estimated the ground state energy at $R = 0.8\text{\AA}$ within $\sim 0.05 \pm 0.05$ Hartree of the exact value without manually correcting for errors, and $\sim -0.005 \pm 0.05$ Hartree after. Previous experiments [27] using trapped ions studying H_2 similarly estimated the ground state energy at $R = 0.75\text{\AA}$ within $\sim 0.04 \pm 0.01$ Hartree of the exact ground state energy. The IBM paper using Richardson Extrapolation for H_2 [17] achieved an accuracy within $\sim 0.005 \pm 0.01$ Hartree of the ground state energy, bootstrapping a larger data set to reduce the effects of sampling noise.

Further research should be performed on larger systems to explore whether these findings hold true for more complex Hamiltonians and ansatz circuits. In order to realize larger applications of quantum computing on near-term devices, a better understanding of error mitigation techniques in the presence of sampling noise is needed. If current techniques fail on small scales, then they are unlikely to work on larger systems with deeper circuits and more complicated error models. How error mitigation techniques such as zero noise extrapolation interface with different qubit architectures, existing quantum algorithms, and other error mitigation techniques will be crucial going forward.

VI. ACKNOWLEDGEMENTS

The authors would like to thank Kenneth Rudinger and Andrew Baczewski from Sandia National Labs for their valuable comments and insight.

This project was funded by the U.S. Department of Energy, Office of Science, Office of Advanced Scientific Computing Research Quantum Testbed Program. Sandia National Laboratories is a multi-mission laboratory managed and operated by National Technology and Engineering Solutions of Sandia, LLC, a wholly owned subsidiary of Honeywell International Inc., for the U.S. Department of Energy's National Nuclear Security Admini-

[1] Peter W. Shor. Polynomial-time algorithms for prime factorization and discrete logarithms on a quantum computer. *SIAM Journal on Computing*, 26(5):1484–1509, Oct 1997. ISSN 1095-7111. doi: 10.1137/s0097539795293172. URL <http://dx.doi.org/10.1137/S0097539795293172>.

[2] Seth Lloyd. Universal quantum simulators. *Science*, 273(5278):1073–1078, 1996. ISSN 00368075, 10959203. URL <http://www.jstor.org/stable/2899535>.

[3] Yudong Cao, Jonathan Romero, Jonathan P. Olson, Matthias Degroote, Peter D. Johnson, Mária Kieferová, Ian D. Kivlichan, Tim Menke, Borja Peropadre, Nicolas P. D. Sawaya, and et al. Quantum chemistry in the age of quantum computing. *Chemical Reviews*, 119(19):10856–10915, Aug 2019. ISSN 1520-6890. doi: 10.1021/acs.chemrev.8b00803. URL <http://dx.doi.org/10.1021/acs.chemrev.8b00803>.

[4] Sam McArdle, Suguru Endo, Alan Aspuru-Guzik, Simon C Benjamin, and Xiao Yuan. Quantum computational chemistry. *Reviews of Modern Physics*, 92(1):015003, 2020.

[5] Alán Aspuru-Guzik, Anthony D. Dutoi, Peter J. Love, and Martin Head-Gordon. Simulated quantum computation of molecular energies. *Science*, 309:1704–1707, 2005. doi:10.1126/science.1113479.

[6] John Preskill. Quantum computing in the nisq era and beyond. *Quantum*, 2:79, Aug 2018. ISSN 2521-327X. doi:10.22331/q-2018-08-06-79. URL <http://dx.doi.org/10.22331/q-2018-08-06-79>.

[7] Sergio Boixo, Sergei V. Isakov, Vadim N. Smelyanskiy, Ryan Babbush, Nan Ding, Zhang Jiang, Michael J. Bremner, John M. Martinis, and Hartmut Neven. Characterizing quantum supremacy in near-term devices. *Nature Physics*, 14(6):595–600, Apr 2018. ISSN 1745-2481. doi:10.1038/s41567-018-0124-x. URL <http://dx.doi.org/10.1038/s41567-018-0124-x>.

[8] Scott Aaronson and Lijie Chen. Complexity-theoretic foundations of quantum supremacy experiments, 2016.

[9] Edwin Pednault, John A. Gunnels, Giacomo Nannicini, Lior Horesh, Thomas Magerlein, Edgar Solomonik, Erik W. Draeger, Eric T. Holland, and Robert Wisnieff. Pareto-efficient quantum circuit simulation using tensor contraction deferral, 2020.

[10] Frank Arute, Kunal Arya, Ryan Babbush, Dave Bacon, Joseph C Bardin, Rami Barends, Rupak Biswas, Sergio Boixo, Fernando GSL Brandao, David A Buell, et al. Quantum supremacy using a programmable superconducting processor. *Nature*, 574(7779):505–510, 2019.

[11] Susan M. Clark, Daniel Lobser, Melissa Revelle, Christopher G. Yale, David Bossert, Ashlyn D. Burch, Matthew N. Chow, Craig W. Hogle, Megan Ivory, Jessica Pehr, Bradley Salzbrenner, Daniel Stick, William Sweatt, Joshua M. Wilson, Edward Winrow, and Peter Maunz. Engineering the quantum scientific computing open user testbed (qscout): Design details and user guide. *IEEE Transactions on Quantum Engineering*, 2021.

[12] K. Wright, K. M. Beck, S. Debnath, J. M. Amini, Y. Nam, N. Grzesiak, J.-S. Chen, N. C. Pisenti, M. Chmielewski, C. Collins, K. M. Hudek, J. Mizrahi, J. D. Wong-Campos, S. Allen, J. Apisdorf, P. Solomon, M. Williams, A. M. Ducore, A. Blinov, S. M. Kreikeimeier, V. Chaplin, M. Keesan, C. Monroe, and J. Kim. Benchmarking an 11-qubit quantum computer. *Nature Communications*, 10(1), nov 2019. doi: 10.1038/s41467-019-13534-2. URL <https://doi.org/10.1038%2Fs41467-019-13534-2>.

[13] Rigetti systems. <https://qcs.rigetti.com/qpus>. Accessed: 10/31/23.

[14] Youngseok Kim, Christopher J Wood, Theodore J Yoder, Seth T Merkel, Jay M Gambetta, Kristan Temme, and Abhinav Kandala. Scalable error mitigation for noisy quantum circuits produces competitive expectation values. *Nature Physics*, pages 1–8, 2023.

[15] Zhenyu Cai, Ryan Babbush, Simon C Benjamin, Suguru Endo, William J Huggins, Ying Li, Jarrod R McClean, and Thomas E O’Brien. Quantum error mitigation. *arXiv preprint arXiv:2210.00921*, 2022.

[16] Kristan Temme, Sergey Bravyi, and Jay M. Gambetta. Error mitigation for short-depth quantum circuits. *Physical Review Letters*, 119(18), Nov 2017. ISSN 1079-7114. doi:10.1103/physrevlett.119.180509. URL <http://dx.doi.org/10.1103/PhysRevLett.119.180509>.

[17] Abhinav Kandala, Kristan Temme, Antonio D. Córcoles, Antonio Mezzacapo, Jerry M. Chow, and Jay M. Gambetta. Error mitigation extends the computational reach of a noisy quantum processor. *Nature*, 567(7749):491–495, Mar 2019. ISSN 1476-4687. doi: 10.1038/s41586-019-1040-7. URL <http://dx.doi.org/10.1038/s41586-019-1040-7>.

[18] O. Shehab, K. Landsman, Y. Nam, D. Zhu, N. M. Linke, M. Keesan, R. C. Pooser, and C. Monroe. Toward convergence of effective-field-theory simulations on digital quantum computers. *Phys. Rev. A*, 100:062319, Dec 2019. doi:10.1103/PhysRevA.100.062319. URL <https://link.aps.org/doi/10.1103/PhysRevA.100.062319>.

[19] Michael Foss-Feig, Stephen Ragole, Andrew Potter, Joan Dreiling, Caroline Figgatt, John Gaebler, Alex Hall, Steven Moses, Juan Pino, Ben Spaun, Brian Neyenhuis, and David Hayes. Entanglement from tensor networks on a trapped-ion quantum computer. *Phys. Rev. Lett.*, 128:150504, Apr 2022. doi: 10.1103/PhysRevLett.128.150504. URL <https://link.aps.org/doi/10.1103/PhysRevLett.128.150504>.

[20] Alberto Peruzzo, Jarrod McClean, Peter Shadbolt, Man-Hong Yung, Xiao-Qi Zhou, Peter J Love, Alán Aspuru-Guzik, and Jeremy L O’Brien. A variational eigenvalue solver on a photonic quantum processor. *Nature communications*, 5:4213, 2014.

[21] Jarrod R McClean, Jonathan Romero, Ryan Babbush, and Alán Aspuru-Guzik. The theory of variational hybrid quantum-classical algorithms. *New Journal of Physics*, 18(2):023023, 2016.

[22] Ying Li and Simon C. Benjamin. Efficient variational quantum simulator incorporating active error minimization. *Physical Review X*, 7(2), jun 2017. doi: 10.1103/physrevx.7.021050.

[23] Tudor Giurgica-Tiron, Yousef Hindy, Ryan LaRose, Andrea Mari, and William J. Zeng. Digital zero noise extrapolation for quantum error mitigation. *2020 IEEE International Conference on Quantum Computing and Engineering (QCE)*, Oct 2020. doi: 10.1109/qce49297.2020.00045. URL <http://dx.doi.org/10.1109/QCE49297.2020.00045>.

[24] L. F. Richardson. IX. the approximate arithmetical solution by finite differences of physical problems involving differential equations, with an application to the stresses in a masonry dam. *Philosophical Transactions of the Royal Society of London. Series A, Containing Papers of a Mathematical or Physical Character*, 210(459-470): 307–357, January 1911. doi:10.1098/rsta.1911.0009. URL <https://doi.org/10.1098/rsta.1911.0009>.

[25] Oliver G Maupin, Andrew D Baczewski, Peter J Love, and Andrew J Landahl. Variational quantum chemistry programs in jaqlapaq. *Entropy*, 23(6):657, 2021.

[26] Jarrod R. McClean, Kevin J. Sung, Ian D. Kivlichan, Yudong Cao, Chengyu Dai, E. Schuyler Fried, Craig Gidney, Brendan Gimby, Pranav Gokhale, Thomas Häner, Tarini Hardikar, Vojtěch Havlíček, Oscar Higgott, Cupjin Huang, Josh Izaac, Zhang Jiang, Xinle Liu, Sam McArdle, Matthew Neeley, Thomas O’Brien, Bryan O’Gorman, Isil Ozfidan, Maxwell D. Radin, Jhonathan Romero, Nicholas Rubin, Nicolas P. D. Sawaya, Kanav Setia, Sukin Sim, Damian S. Steiger, Mark Steudtner, Qiming Sun, Wei Sun, Daochen Wang, Fang Zhang, and Ryan Babbush. Openfermion: The electronic structure package for quantum computers, 2017.

[27] Cornelius Hempel, Christine Maier, Jonathan Romero, Jarrod McClean, Thomas Monz, Heng Shen, Petar Jurcevic, Ben P. Lanyon, Peter Love, Ryan Babbush, Alán Aspuru-Guzik, Rainer Blatt, and Christian F. Roos. Quantum chemistry calculations on a trapped-ion quantum simulator. *Phys. Rev. X*, 8:031022, Jul 2018. doi: 10.1103/PhysRevX.8.031022. URL <https://link.aps.org/doi/10.1103/PhysRevX.8.031022>.

[28] Mark R Hoffmann and Jack Simons. A unitary multi-configurational coupled-cluster method: Theory and applications. *The Journal of chemical physics*, 88(2):993–1002, 1988.

[29] Rodney J Bartlett, Stanislaw A Kucharski, and Jozef Noga. Alternative coupled-cluster ansätze ii. the unitary coupled-cluster method. *Chemical physics letters*, 155(1): 133–140, 1989.

[30] Andrew G Taube and Rodney J Bartlett. New perspectives on unitary coupled-cluster theory. *International journal of quantum chemistry*, 106(15):3393–3401, 2006.

[31] Gaurav Harsha, Toru Shiozaki, and Gustavo E Scuseria. On the difference between variational and unitary coupled cluster theories. *The Journal of chemical physics*, 148(4):044107, 2018.

[32] Peter JJ O’Malley, Ryan Babbush, Ian D Kivlichan, Jonathan Romero, Jarrod R McClean, Rami Barends, Julian Kelly, Pedram Roushan, Andrew Tranter, Nan Ding, et al. Scalable quantum simulation of molecular energies. *Physical Review X*, 6(3):031007, 2016.

[33] M. J. D. Powell. *A Direct Search Optimization Method That Models the Objective and Constraint Functions by Linear Interpolation*, pages 51–67. Springer Netherlands, Dordrecht, 1994. ISBN 978-94-015-8330-5. doi: 10.1007/978-94-015-8330-5_4. URL https://doi.org/10.1007/978-94-015-8330-5_4.

[34] Pauli Virtanen, Ralf Gommers, Travis E. Oliphant, Matt Haberland, Tyler Reddy, David Cournapeau, Evgeni Burovski, Pearu Peterson, Warren Weckesser, Jonathan Bright, Stéfan J. van der Walt, Matthew Brett, Joshua Wilson, K. Jarrod Millman, Nikolay Mayorov, Andrew R. J. Nelson, Eric Jones, Robert Kern, Eric Larson, C J Carey, İlhan Polat, Yu Feng, Eric W. Moore, Jake VanderPlas, Denis Laxalde, Josef Perktold, Robert Cimrman, Ian Henriksen, E. A. Quintero, Charles R. Harris, Anne M. Archibald, António H. Ribeiro, Fabian Pedregosa, Paul van Mulbregt, and SciPy 1.0 Contributors. SciPy 1.0: Fundamental Algorithms for Scientific Computing in Python. *Nature Methods*, 17:261–272, 2020. doi:10.1038/s41592-019-0686-2.

[35] E. F. Dumitrescu, A. J. McCaskey, G. Hagen, G. R. Jansen, T. D. Morris, T. Papenbrock, R. C. Pooser, D. J. Dean, and P. Lougovski. Cloud quantum computing of an atomic nucleus. *Phys. Rev. Lett.*, 120:210501, May 2018. doi:10.1103/PhysRevLett.120.210501. URL <https://link.aps.org/doi/10.1103/PhysRevLett.120.210501>.

[36] Andre He, Benjamin Nachman, Wibe A. de Jong, and Christian W. Bauer. Zero-noise extrapolation for quantum-gate error mitigation with identity insertions. *Physical Review A*, 102(1), jul 2020. doi: 10.1103/physreva.102.012426. URL <https://doi.org/10.1103/2physreva.102.012426>.

[37] Swarnadeep Majumder, Christopher G. Yale, Titus D. Morris, Daniel S. Lobser, Ashlyn D. Burch, Matthew N. H. Chow, Melissa C. Revelle, Susan M. Clark, and Raphael C. Pooser. Characterizing and mitigating coherent errors in a trapped ion quantum processor using hidden inverses. *Quantum*, 7:1006, may 2023. doi: 10.22331/q-2023-05-15-1006. URL <https://doi.org/10.22331/2Fq-2023-05-15-1006>.

[38] Abhinav Kandala, Antonio Mezzacapo, Kristan Temme, Maika Takita, Markus Brink, Jerry M. Chow, and Jay M. Gambetta. Hardware-efficient variational quantum eigensolver for small molecules and quantum magnets. *Nature*, 549(7671):242–246, Sep 2017. ISSN 1476-4687. doi:10.1038/nature23879. URL <http://dx.doi.org/10.1038/nature23879>.

[39] Alexis Ralli, Peter J. Love, Andrew Tranter, and Peter V. Coveney. Implementation of measurement reduction for the variational quantum eigensolver. *Phys. Rev. Res.*, 3:033195, Aug 2021. doi: 10.1103/PhysRevResearch.3.033195. URL <https://link.aps.org/doi/10.1103/PhysRevResearch.3.033195>.

Appendix A: Error Analysis

The output of s samples of M Hamiltonian terms is a set of sM variables $p_j^{(k)}$ where $1 \leq j \leq M$ and $1 \leq k \leq s$. We consider the Hamiltonian terms to label the rows of this array of data and the samples to label the columns. The standard analysis of VQE data involves summing the samples along the rows to obtain an estimate of the expectation value of each term in the Hamiltonian. These estimates are then combined with the coefficients of the Hamiltonian to obtain an estimate of the energy expectation value for the Hamiltonian [21]. The error on this

estimate is obtained by standard error propagation from the uncertainties on the terms. In this work, we calculate the standard error on the mean of our estimates of the energy expectation value by instead summing the output samples along the columns (re: Hamiltonian terms weighted by coefficients) as implemented in [39]. Doing so gives us a distribution of s energy estimates derived from singular samples with its own mean and variance. This mean is the same estimate as in the standard analysis.

We report percentage relative errors ϵ of our measured expectation values $E_{measured}$ compared to the theoretical exact ground state energy E_{theory} as follows:

$$\epsilon = 100 * \frac{|E_{measured} - E_{theory}|}{E_{theory}} \quad (A1)$$

with accompanying percentage uncertainty σ calculated from the standard error of the mean of our measured expectation values $\sigma_{measured}$:

$$\sigma = 100 * \frac{\sigma_{measured}}{E_{theory}} \quad (A2)$$

When comparing an extrapolated expectation value to an estimate from an unaltered circuit, we report the relative difference as a percentage:

$$\delta = 100 * \frac{|E_{extrapolated} - E_{theory}|}{|E_{unaltered} - E_{theory}|} \quad (A3)$$

where a value less than 100% indicates that the extrapolated estimate has less error than the non-error-mitigated estimate and a value greater than 100% indicates that the extrapolated estimate has introduced more error.